

## Article

# Sustainable Integration of Zinc Oxide Nanoparticles: Enhancing Properties of Poly( $\epsilon$ -Caprolactone) Electrospun Nanofibers and Cast Films

Johar Amin Ahmed Abdullah <sup>1,\*</sup>, José J. Benítez <sup>2</sup>, Antonio Guerrero <sup>1</sup> and Alberto Romero <sup>3</sup>

<sup>1</sup> Departamento de Ingeniería Química, Escuela Politécnica Superior, Universidad de Sevilla, 41011 Sevilla, Spain; aguerrero@us.es

<sup>2</sup> Instituto de Ciencia de Materiales de Sevilla, Centro Mixto CSIC, Universidad de Sevilla, 41092 Sevilla, Spain; benitez@icmse.csic.es

<sup>3</sup> Departamento de Ingeniería Química, Facultad de Química, Universidad de Sevilla, 41012 Sevilla, Spain; alromero@us.es

\* Correspondence: jabdullah@us.es; Tel.: +34-954-557-179

**Abstract:** This study investigated the impact of adding zinc oxide nanoparticles (ZnO-NPs) to electrospun membranes and cast films made of poly( $\epsilon$ -caprolactone) (PCL). The physicochemical, mechanical, and morphological properties of the samples were analyzed. Physicochemical parameters included water contact angle (WCA), water vapor transmission rate (WVTR), permeance, water vapor permeability (WVP), light transmission ( $T_{600}$ ), and transparency (T). Mechanical properties, such as maximum stress ( $\sigma_{max}$ ), elongation ( $\epsilon_{max}$ ), and Young's modulus (MPa), were also evaluated. Morphological properties were analyzed in terms of thickness, dispersion, and surface roughness (measured by the arithmetic ( $R_a$ ) and quadratic ( $R_q$ ) averages). The crystallinity and melting point, as well as the functional DPPH $^{\bullet}$  scavenging percentage (SP%), were also studied. The results showed that adding 1 wt% ZnO-NPs improved the water barrier properties of PCL membranes and films, increasing WCA by 1%–6% and decreasing WVTR by 11%–19%, permeance by 34%–20%, and WVP by 4%–11%, respectively. The  $T_{600}$  values of PCL/ZnO-NPs membranes and films were 2–3 times lower than those of neat PCL samples, indicating improved optical properties. The mechanical properties of the composite membranes and films also improved, with  $\sigma_{max}$  increasing by 56%–32% and Young's modulus increasing by 91%–95%, while  $\epsilon_{max}$  decreased by 79%–57%. The incorporation of ZnO-NPs also increased the thickness and surface roughness of the samples. The SP% of PCL/ZnO-NPs increased by almost 69%, demonstrating the beneficial effects of ZnO-NPs on the system. These findings suggest that incorporating ZnO-NPs into PCL membranes and films can enhance their properties, making them well suited for various applications, such as those within the realm of materials science and nanotechnology.



**Citation:** Abdullah, J.A.A.; Benítez, J.J.; Guerrero, A.; Romero, A. Sustainable Integration of Zinc Oxide Nanoparticles: Enhancing Properties of Poly( $\epsilon$ -Caprolactone) Electrospun Nanofibers and Cast Films. *Coatings* **2023**, *13*, 1665. <https://doi.org/10.3390/coatings13101665>

Academic Editor: Florina Branzoi

Received: 25 August 2023

Revised: 18 September 2023

Accepted: 20 September 2023

Published: 22 September 2023



**Copyright:** © 2023 by the authors. Licensee MDPI, Basel, Switzerland. This article is an open access article distributed under the terms and conditions of the Creative Commons Attribution (CC BY) license (<https://creativecommons.org/licenses/by/4.0/>).

## 1. Introduction

Electrospinning (ES) is one of the most novel and effective technologies used to produce nano- and  $\mu$ -scale fibers [1]. The process involves accelerating a jet of charged polymer solution under a carefully induced electric field to form an interconnected network of nanofibers on a drum collector surface [2–4]. ES can produce nanofibers or nanofiber mats from several polymers and/or polymer blends [5,6] with the incorporation of several metallic and non-metallic oxide nanomaterials [7–9] or molecules with functional properties into systems [10–12]. Material composition and applications play a significant role in the performance of the nanofibers, for example, in biomedical applications [13–15], gas and fluid filtration [16–18], energy harvesting and storage, such as the production of hydrogen

(H<sub>2</sub>) [19–21], oil–water separation, water purification, and environmental protection [22–25], catalytic applications [26–28], food packaging [29], protein adsorption [30], waterproof and breathable clothing [31], sensors [32], optical applications [33], and lithium-ion batteries [34].

Among the well-known aliphatic polymers, polycaprolactone (PCL) has been utilized extensively for producing a wide range of synthetic nanofibers, due to its outstanding characteristics, since it is biodegradable, biocompatible, bioresorbable, hydrophobic, easy to process, and non-toxic [2,24]. PCL exhibits exceptional solubility in a wide range of solvents, allowing for facile and efficient electrospinning processes. Its ability to form uniform and fine nanofibers makes it an excellent choice for various applications. These processing advantages further solidify PCL's position as a valuable material in the realm of electrospinning [3]. Furthermore, electrospun PCL nanofibers may also display higher levels of hydrophilicity and biocompatibility if they are treated with surface coatings, poly-dopamine, plasma, alkali, copolymer blends, and polymer grafting, thereby providing an attractive option for several applications [35–38]. Regarding packaging purposes, particular attention should be devoted to containment, protection, convenience, and communication. A significant loss of food's economic value occurs when its lipids deteriorate during storage due to oxygen spoilage and microorganisms. A product's shelf life is significantly reduced by oxidation, which depletes its nutritional value and causes the appearance of unpleasant odors, flavors, and pigments. As rancidity and the aforementioned alterations are caused by free radical molecules, food packaging designers are continually developing new methods to prevent and reduce products' auto-oxidation [39].

This problem may be solved by the incorporation of nanoparticles into polymer-based materials, due to the highly efficient antioxidant and antimicrobial properties of nanoparticles [6,40,41]. Therefore, in recent years, the use of metal nanoparticles in combination with polymer nanofibers (metal–polymer nanocomposites) has generated a great deal of interest due to the synergistic combination of optical, electrical, specific, unique, functional, and catalytic characteristics. Several factors contribute to this, including the high surface area of polymer nanofibers and the interaction between metal nanoparticles and polymer nanofibers. Accordingly, nanoparticles of metal oxides, including nanofillers, are introduced into films and nanofiber-based polymers to enhance their properties [42–44]. Furthermore, the nature of PCL interaction with nanoparticles has been demonstrated in several studies [45,46]. Among the best-known nanoparticles, inorganic semiconducting zinc oxide nanoparticles (ZnO-NPs) have found use in various applications due to their diverse chemical and physical characteristics [47].

Nevertheless, owing to the readily agglomerating properties of nanoparticles and the high viscosity of polymer solutions, mechanical mixing of metal nanoparticles into the dissolved polymer matrix results in an inhomogeneous dispersion of particles within the highly viscous matrix [6,40,41,48,49]. DMF (N,N-dimethylformamide) has been successfully employed to reduce metal ions (M<sup>+</sup>) to zero-valent metal, thereby reducing the formation of aggregates or agglomerates [50]. Despite this, the aforementioned studies did not provide sufficient information regarding nanoparticle incorporation and their effect on physicochemical (including hydrophobicity, water vapor permeability, and optical properties), mechanical, and morphological characteristics. The majority of these studies did not address the functional properties of nanoparticles that contribute to improving the antioxidant properties of membranes and films in order to extend their shelf lives and to prevent autoxidation. Therefore, this study primarily contributes to the development of electrospun membranes and cast films containing zinc oxide nanoparticles (ZnO-NPs). To this end, PCL (10% *w/v* dissolved in chloroform: DMF [9:1]) with 1% (*w/w*) of zinc oxide nanoparticles (ZnO-NPs) was processed via two methods: electrospinning to produce PCL-based electrospun nanofiber membranes and casting to fabricate PCL-based cast films. PCL electrospun membranes and cast films were characterized for their physicochemical, mechanical, morphological and antioxidant properties. According to the results, ZnO-NPs' incorporation significantly improved the properties mentioned above and could be applied to a wide range of applications.

## 2. Materials and Methods

### 2.1. Materials

Polycaprolactone PCL ( $C_6H_{10}O_2)_n$  (with average Mn 80,000; Sigma Aldrich, Saint Louis, MI, USA), DMF ( $CH_3)_2NC(O)H$  (Merck, Darmstadt, Germany), Chloroform (Friedemann Schmidt, Parkwood, Australia), DPPH (2,2-diphenyl-1-picrylhydrazyl), methanol ( $CH_3OH$ ), and gallic acid ( $C_7H_6O_5$ ) were purchased from Sigma Aldrich. The other substances and reagents used in this study were all of analytical grade.

Green synthesized zinc oxide nanoparticles (ZnO-NPs) with an average diameter of 15–20 nm were obtained as described in an earlier study [51].

### 2.2. Electrospun Membrane and Cast Film Processing

Nanofibrous membranes based on electrospun neat PCL (neat PCL) and PCL with ZnO-NPs (PCL/ZnO-NPs) were prepared by solution electrospinning according to prior studies with minor modifications [2,51]. Firstly, 1 g of PCL was carefully dissolved in 10 mL of chloroform/DMF (9:1 *v/v*) and stirred continuously at room temperature for 24 h to prepare the electrospinning dope and the film-forming solution. Then, ZnO-NPs (1.0 *w/w* of the dry PCL) were dispersed in the PCL solution for 2 h using an ultrasound bath at 50 Hz frequency and 0.1 kW sonication power (Ultrasounds, J.P Selecta, S.A., Barcelona, Spain). In the case of the electrospinning process, 10 mL of PCL solution was electrospun through an electrospinning machine (BioInicia, Fluidnatek LE-50 setup, Valencia, Spain) for 2 h at 12 kV voltage, 13 cm distance between the needle and the collector (rotating drum collector, 200 rpm) and 0.9 mL/h feed rate on an aluminum foil. In the case of the films, 10 mL of the same solution was cast into glass Petri plates (80 × 17 mm) and dried at room temperature for 48 ± 24 h. The electrospun membranes and cast films were carefully removed after drying and stored for further use and analysis.

## 3. Characterization Techniques

### 3.1. Water Contact Angle (WCA)

WCAs of the electrospun membranes and cast films were assessed with an Optical Tensiometer (Attension TL100, KSV, Helsinki, Finland) to evaluate the hydrophobicity of their surfaces as described in prior studies [51,52]. Briefly, ≈2 μL of distilled water was dropped onto a horizontally level surface membrane or film (1 cm<sup>2</sup>) using a μ-syringe and allowing stabilization.

The WCA was calculated from both the left and right sides of the drop contour; values differing more than 2° were rejected.

### 3.2. Water Vapor Permeability (WVP)

WVP of membranes and films were measured based on ASTM E96 methodology [53], and as described in [52], using Equation (1):

$$WVP = P \times t = \frac{WVTR}{\Delta p} \times t = \frac{\alpha}{AS(RH_1 - RH_2)} \times t \quad (1)$$

where  $P$  refers to the permeance (g/h·m<sup>2</sup>·Pa) and thickness ( $t$ , m) of the membrane or film, WVTR( $\alpha/A$ ) is the water vapor transmission rate (g/h·m<sup>2</sup>),  $\alpha$  is the slope of the linear regime of the weight loss vs. time curve,  $A$  refers to the permeation area (cm<sup>-2</sup>), and  $\Delta p = S(RH_1 - RH_2)$  is the water vapor gradient ( $S = 2646$  Pa) at 22° between the water-exposed surface ( $RH_1 = 1$ ) and chamber-exposed surface ( $RH_2 = 0$ ).

### 3.3. Light Transmission ( $T_{600\%}$ ) and Transparency ( $T$ )

The different membranes and films were evaluated for their optical properties through transmittance and transparency measurements, using a UV-vis spectrophotometer (Model 8451A, Hewlett Packard Co., Spring, TX, USA) as reported in previous studies [51,54].

Briefly, the transmittance% of the samples ( $1 \times 2 \text{ cm}^2$ ) was read at 600 nm ( $T_{600\%}$ ), and the transparency (T) was calculated from the ( $T_{600\%}$ ) fraction according to Equation (2) [55]:

$$T = \frac{-\log T_{600}}{t} \quad (2)$$

where  $t$  is the thickness of the sample (mm).

### 3.4. Mechanical Properties

The mechanical characteristics of the different membranes and films were evaluated following the ISO 527-3:2019 standard [52,56]. As a result of this test, the maximum stress ( $\sigma_{\max}$ ), elongation ( $\epsilon_{\max}$ ), and Young's modulus (MPa) of the samples were determined.

### 3.5. Optical Microscopy

The morphological characteristics of the different membranes and films were assessed using a high-precision zoom lens (Edmund Optics, Barrington, NJ, USA) calibrated with a 22GA needle. In addition, measurements of specimen diameters and thicknesses were assessed using ImageJ (free software v.1.53q; National Institutes of Health, Bethesda, MD, USA).

### 3.6. Scanning Electron Microscopy (SEM)

The morphological characteristics of the different membranes and films were assessed using SEM (Zeiss EVO microscope, Pleasanton, CA, USA) as described in an earlier study [57]. In brief, SEM analysis was conducted at a 10 kV acceleration voltage and 3 KX magnification. In addition, measurements of specimen diameters and thicknesses were assessed using ImageJ (free software v.1.53q; National Institutes of Health, Bethesda, MD, USA).

### 3.7. Transmission Electron Microscopy (TEM)

TEM analysis was performed at 200 kV to confirm the morphological properties of the different membranes and films (Talos S200 microscope, Field Electron, and Ion Company, FEI, San Juan Capistrano, CA, USA). A further assessment was conducted using ImageJ (free software v.1.53q; National Institutes of Health, Bethesda, MD, USA).

### 3.8. Confocal Microscopy

The surface roughness profiles of different PCL electrospun membranes and cast films were measured using a Confocal-Interferometric Optical Microscope (Sensofar S-NEOX, Sky Tech, Bukit Batok, Singapore) with a Robust Gaussian filter at an amplitude of 8  $\mu\text{m}$  and magnification of 50–150 $\times$  (ISO 4287) [58]. The samples were coated with a 10 nm platinum thin layer to allow for better light reflection. Accordingly, surface roughness was determined by both the arithmetic (Ra) and quadratic (Rq) averages using SensoMAP Premium (v.7.4.8114; SENSOFAR METROLOGY, Barcelona, Spain).

### 3.9. X-ray Diffraction (XRD)

Diffractograms of electrospun membranes and cast films were recorded at room conditions between  $2\theta (\circ) = 5\text{--}70^\circ$  using an X'Pert Pro (PANalytical, Malvern, UK) diffractometer with CuK $\alpha$  radiation. Diffractograms were fitted using the Gaussian function ( $R^2 = 0.98$ ) and crystallinity (CrI%) was determined according to Equation (3) [59]:

$$\text{CrI}(\%) = \frac{\text{ACP}}{\text{CPA} + \text{AM}} \times 100 \quad (3)$$

where ACP is the area of crystalline peaks, CPA is the crystalline peak area, and AM is the amorphous area.

### 3.10. Differential Scanning Calorimetry (DSC)

Thermograms were measured using a differential scanning calorimeter (Q-20, TA Instruments, New Castle, DE, USA) under nitrogen flow (50 mL/min) in the  $-70\text{--}120^\circ\text{C}$  range at

10 °C/min. Samples were previously dried in a desiccator for 48 h. The crystallization percentage or crystallinity degree  $\chi_c$ (%) of the polymer is calculated from the melting enthalpy  $\Delta H_f$ , based on the melting or fusion heat according to Equation (4) [60].

$$\chi_c(\%) = \frac{\Delta H_f}{\Delta H_{f100\%}} \times 100 \quad (4)$$

$\Delta H_{f100\%}$  is the melting enthalpy of the 100% crystalline form of PCL (J/g). The  $\Delta H_{f100\%}$  value has been reported to be 142 J/g [61], 139.3 J/g [62], 136 J/g [63], and 135 J/g [60,64]. Here, the value of 139.5 J/g was adopted.

### 3.11. Antioxidant Activity (DPPH<sup>•</sup> Scavenging Activity)

The antioxidant activity of the membrane and film solution (neat PCL and PCL/ZnO-NPs solution) was assessed using the DPPH<sup>•</sup> scavenging test as reported in a previous study [54]. Briefly, 1 mL of membrane or film-forming solution was mixed with 1 mL of methanolic DPPH free radical solution (40 ppm) using gallic acid as a positive control. After 30 min incubation, the absorbance of the samples was measured at 517 nm with a spectrophotometer. Finally, the DPPH<sup>•</sup> scavenging percentage (SP%) was determined according to Equation (5).

$$SP(\%) = ((ADPPH^{\bullet} - ADPPH)/ADPPH^{\bullet}) \times 100 \quad (5)$$

where ADPPH<sup>•</sup> is the absorbance of raw DPPH<sup>•</sup> solution and ADPPH is the absorbance of scavenged DPPH by the membrane and film solution.

### 3.12. Statistical Analysis

The samples were subjected to at least three measurements. A summary of the results is provided as an  $M \pm SD$  (a mean value  $\pm$  standard deviation). The significance of the difference between measurements was evaluated using IBM SPSS software (IBM Corp., Armonk, NY, USA. Released 2019. IBM SPSS Statistics for Windows, Version 26.0. Armonk, NY, USA, IBM Corp.) and one-way ANOVA ( $p < 0.05$ ).

## 4. Results

### 4.1. WCA

The membrane and film surface wettability and hydrophobicity/hydrophilicity and the effect of nanoparticle incorporation were evaluated using WCA measurements [55,65]. The WCAs of neat electrospun and cast PCL, as well as their composite membranes and films (PCL/ZnO-NPs), are depicted in Figure 1 and summarized in Table 1. Regarding the processing, the neat PCL electrospun nanofibrous membrane exhibited a more hydrophobic surface than the cast film with  $WCA = 122.7 \pm 0.9^\circ$  vs.  $WCA = 114.8 \pm 0.2^\circ$ . As a result, the porous and free spaces within the electrospun membrane may be smaller than those within cast film, resulting in well-connected networks [66]. It was determined that PCL electrospun (12% *w/v* in acetic-formic acid mixture 3:7) had a WCA value of  $118^\circ$  [67]. With the ZnO-NPs incorporation, the WCA of PCL/ZnO-NPs electrospun membranes did not significantly increase (Table 1), but they did show a significant increase in the PCL/ZnO-NPs cast film from  $114.8 \pm 0.2$  to  $122.2^\circ$  (Table 1,  $p < 0.05$ ), which is consistent with the hydrophobic nature of PCL (due to the presence of  $CH_2$  groups in the main chain) and the hydrophobicity of ZnO-NPs [68]. The ZnO-NPs enhanced the hydrophobic behavior due to several interactions, including ionic and hydrogen bonds, resulting in the formation of strong across-linked networks or structures [69]. The surface roughness may also increase due to the presence of nanoparticles, which increases the chemical effect of the nanoparticles on the composite membrane, thereby increasing the film's hydrophobicity [70]. PCL electrospun membranes and cast films prepared in a variety of solvent systems were previously reported to have similar WCA values [71–75].

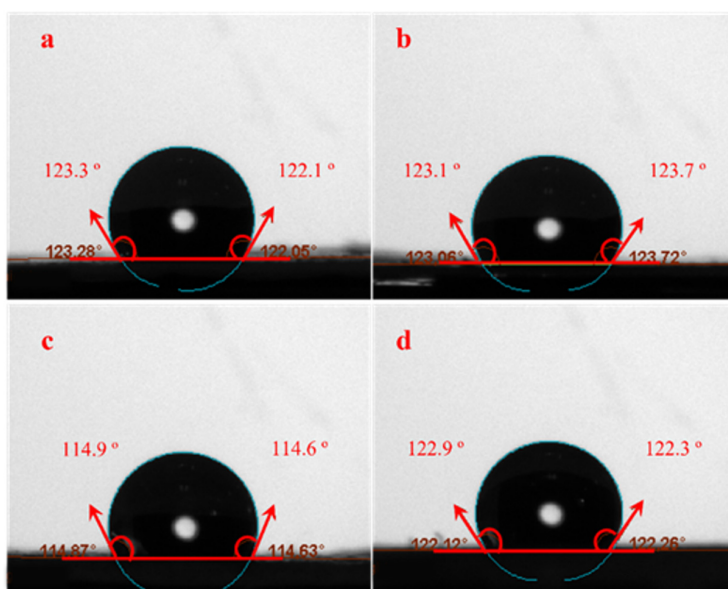


**Figure 1.** Water contact angle photographs of the different PCL electrospun membranes and cast films: (a) neat PCL electrospun membranes, (b) PCL/ZnO-NPs electrospun membranes, (c) neat PCL cast film, and (d) PCL/ZnO-NPs cast films.

**Table 1.** Physicochemical parameters of the different PCL electrospun membranes and cast films.

Samples	Material Incorporated (Concentration)	WCA (°)	WVTR (g/h·m <sup>2</sup> )	Permeance (g/h·m <sup>2</sup> ·Pa) × 10 <sup>-2</sup>	WVP (g·m/h·m <sup>2</sup> ·Pa) × 10 <sup>-7</sup>	T <sub>600</sub> (%)	T
a	Neat PCL nanofibers	-	122.7 ± 0.9 <sup>a</sup>	4.4 ± 0.03 <sup>c</sup>	27.7 ± 0.02 <sup>c</sup>	1.8 ± 0.4 <sup>b</sup>	26.3 ± 0.9 <sup>b</sup>
b	PCL/ZnO-NPs nanofibers	ZnO-NPs (1 wt%)	123.4 ± 0.5 <sup>a</sup>	2.9 ± 0.01 <sup>d</sup>	26.5 ± 0.01 <sup>d</sup>	0.8 ± 0.2 <sup>c</sup>	29.5 ± 0.9 <sup>a</sup>
c	Neat PCL film	-	114.8 ± 0.2 <sup>b</sup>	5.6 ± 0.02 <sup>a</sup>	62.3 ± 0.03 <sup>a</sup>	6.4 ± 1.4 <sup>a</sup>	9.8 ± 0.5 <sup>d</sup>
d	PCL/ZnO-NPs film	ZnO-NPs (1 wt%)	122.2 ± 0.1 <sup>a</sup>	4.5 ± 0.01 <sup>b</sup>	55.0 ± 0.04 <sup>b</sup>	2.1 ± 0.5 <sup>b</sup>	13.0 ± 0.4 <sup>c</sup>

Note: Different superscript letters (a–d) of each column indicate heterogeneity of variances ( $p < 0.05$ ).

#### 4.2. Water Vapor Permeability (WVP)

WVTR (water vapor transmission rate) measurements were conducted to assess the effects of membrane and film processing, as well as the incorporation of zinc oxide nanoparticles. The results of the different parameters, including WVTR, permeance, and WVP means are summarized in Table 1. Accordingly, the neat PCL electrospun nanofibrous membrane exhibited lower WVTR, permeance, and WVP than the cast film. Cast films may exhibit increased permeability due to the more rapid diffusion of water molecules through the contact zones between the circular structures (see Section 4.5). In other words, a less compact structure. As these circular structures are finer, the passage of water molecules may be favored. In contrast, studies have reported that the amorphous structure of electrospun membranes provides better physicochemical properties than the semicrystalline structure [76]. Furthermore, zinc oxide nanoparticles have demonstrated significant reductions in these parameters in both types of processes.

The mean WVP of the neat PCL electrospun membrane was reduced from  $27.7 \pm 0.02$  to  $26.5 \pm 0.01$  ( $\text{g} \cdot \text{m}/\text{h} \cdot \text{m}^2 \cdot \text{Pa}) \times 10^{-7}$ , while the WVP of the cast film decreased from  $62.3 \pm 0.03$  to  $55.0 \pm 0.04$  ( $\text{g} \cdot \text{m}/\text{h} \cdot \text{m}^2 \cdot \text{Pa}) \times 10^{-7}$  with ZnO-NPs incorporation (Table 1,  $p < 0.05$ ).

In the presence of ZnO-NPs, three-dimensional structures may develop, and twisted pathways may be formed along the matrix, which delays the passage of water molecules [75,77–79]. The reason for this is that nanoparticles interact strongly with polymer chains, consuming

hydrophilic groups, which reduces water transmission [80]. Nevertheless, the water vapor permeability of composite membranes or films is affected by several factors, including compaction, crystallinity, hydrophobicity and/or hydrophilicity behavior, nanofiber orientation, roughness, thickness, particle crystallinity, size, and distribution or orientation [71,81,82]. In this regard, ZnO-NPs improved the WVP of the composite PCL electrospun membranes and cast films due to their size and crystalline characteristics. The hydrophobic nanoparticles enhance the hydrophobicity within the polymer matrix by reducing the free hydroxyl groups, increasing their moisture resistance, and decreasing water vapor permeability [83,84].

#### 4.3. Light Transmission ( $T_{600\%}$ ) and Transparency ( $T$ )

Table 1 also summarizes the values of  $T_{600\%}$  and transparency  $T$  for neat electrospun and cast PCL as well as their composite membranes and films (PCL/ZnO-NPs). Figure 2 provides a visual representation of these membranes and films.

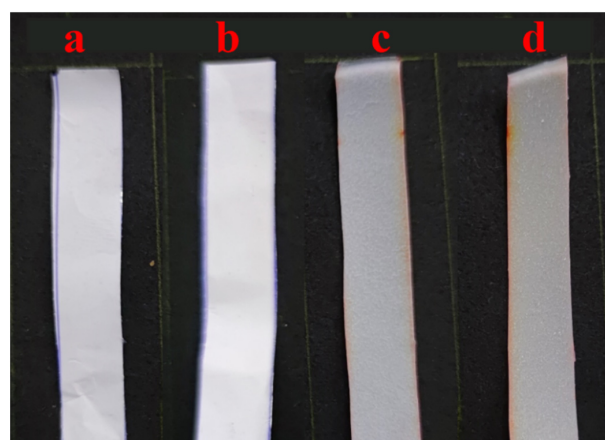


**Figure 2.** The visual appearance of the different PCL electrospun membranes and cast films: (a) neat PCL electrospun membranes, (b) PCL/ZnO-NPs electrospun membranes, (c) neat PCL cast film, and (d) PCL/ZnO-NPs cast film.

In both electrospun membranes and cast films, ZnO-NP incorporation led to a significant decrease in  $T_{600\%}$ , with increases in  $T$  indexes, since the membranes were almost opaque (it was not possible to look through the membrane, Figure 2). As a result, PCL-cast films have the highest transmissions ( $6.4 \pm 1.4\%$ ), which is possibly due to a less compact structure, which allows light to pass through the films. Both electrospun membranes and cast films, when treated with ZnO-NPs, showed a decrease in  $T_{600\%}$  of almost 56 and 66%, respectively, by blocking the free spaces and favoring the compaction between the nanofibers and those present in the film, thereby forming a more closed structure. This resulted in an increase in  $T$  values of approximately 11 and 25%, respectively (Table 2,  $p < 0.05$ ).

**Table 2.** Thickness ( $\mu\text{m}$ ) and mechanical parameters of the different PCL electrospun membranes and cast films.

Sample	Material Incorporated (Concentration)	Thickness ( $\mu\text{m}$ )	$\sigma_{\max}$ (MPa)	$\varepsilon_{\max}$ (mm/mm)	Young's Modulus (MPa)
a	Neat PCL nanofibers	-	$62.7 \pm 0.1^{\text{b}}$	$2.8 \pm 0.0^{\text{d}}$	$3.9 \pm 0.1^{\text{a}}$
b	PCL/ZnO-NPs nanofibers (1 wt%)	$67.5 \pm 0.2^{\text{c}}$	$6.3 \pm 0.1^{\text{a}}$	$0.8 \pm 0.1^{\text{b}}$	$48.6 \pm 0.2^{\text{b}}$
c	Neat PCL film	-	$112.7 \pm 0.1^{\text{d}}$	$2.5 \pm 0.1^{\text{b}}$	$0.7 \pm 0.1^{\text{b}}$
d	PCL/ZnO-NPs film (1 wt%)	$122.1 \pm 0.6^{\text{a}}$	$3.7 \pm 0.2^{\text{b}}$	$0.3 \pm 0.1^{\text{c}}$	$132.7 \pm 1.3^{\text{a}}$

Note: Different superscript letters (a–d) of each column indicate heterogeneity of variances ( $p < 0.05$ ).

Essentially, the presence of crystalline nanoparticle content in the polymer chains hinders their mobility and fills up free spaces in the matrix through dispersion. Therefore, it blocks the passage of light through the system. A variety of polymers blended with other nanoparticles have also produced similar results [55,85–88].

#### 4.4. Mechanical Properties

Figure 3 shows the tensile profile of neat electrospun and cast PCL as well as their composite membranes and films (PCL/ZnO-NPs), with a photograph showing the membrane and film flexibility.

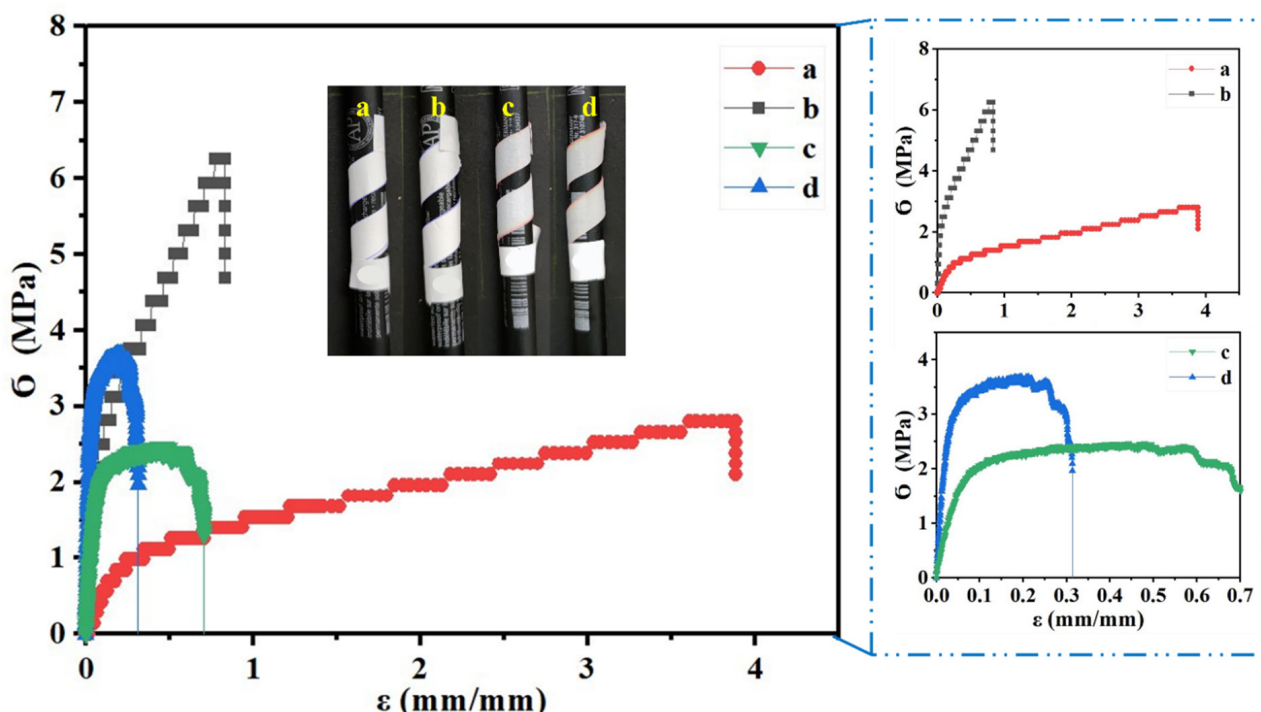


**Figure 3.** Tensile test profile of the different PCL electrospun membranes and cast films: (a) neat PCL electrospun membranes, (b) PCL/ZnO-NPs electrospun membranes, (c) neat PCL cast film, and (d) PCL/ZnO-NPs cast film. The photograph inside with yellow letters illustrates the flexibility of the membrane and film.

A summary of the mechanical parameters is provided in Table 2.

Accordingly, the neat PCL electrospun membranes exhibited the greatest elongation with  $\varepsilon_{\max} \approx 3.9$  mm/mm, whereas the cast films exhibited lower  $\sigma_{\max}$  ( $\approx 2.5$  MPa) and greater Young's modulus ( $\approx 6.5$  MPa) than the neat PCL electrospun membranes ( $\approx 2.8$  MPa and  $\approx 4.3$  MPa, respectively) (Table 2,  $p < 0.05$ ). As the PCL electrospun membranes and films were blended with ZnO-NPs (1% *w/w*), increases in  $\sigma_{\max}$  and Young's modulus were observed, as well as decreases in  $\varepsilon_{\max}$ . The nanofiber structure seems to favor sliding and orientation in the direction of stress, resulting in high elongation and low modulus. Through the incorporation of ZnO-NPs, the nanofibers intertwine and prevent slippage, resulting in an increase in modulus, a decrease in breaking stress, and a decrease in elongation. The cast films also exhibit the same pattern.

For PCL/ZnO-NPs electrospun membranes, the  $\sigma_{\max}$  and Young's modulus increased by about 56 and 91%, whereas these parameters increased by about 32 and 95%, respectively, in the PCL/ZnO-NPs cast film system. Similar increases in these parameters have been observed in studies of similar designs [89]. The mechanical properties may be affected by several parameters, including processing conditions, mechanical procedure, thickness, etc. Therefore, the consequence of the nanoparticle dispersion as an immiscible content within the polymer matrix, hydrogen bonds may form between the nanoparticles and the

polymer chains, resulting in nonhomogeneous networks in the matrix, thereby enhancing the mechanical properties of the membranes and the films [85,90]. Moreover, a reduction in  $\varepsilon_{\max}$  was observed over ZnO-NPs reinforcement, suggesting that the incorporation of solid materials into the polymer matrix may enhance the film thickness and decrease surface cohesion forces [85,91]. Several investigations have shown that nanoparticles have a similar effect on the mechanical properties of polymers [54,92].

#### 4.5. Optical Properties

A morphological and microstructural illustration of neat electrospun, cast PCL, and their composite membranes and films (PCL/ZnO-NPs) is shown in Figure 4.

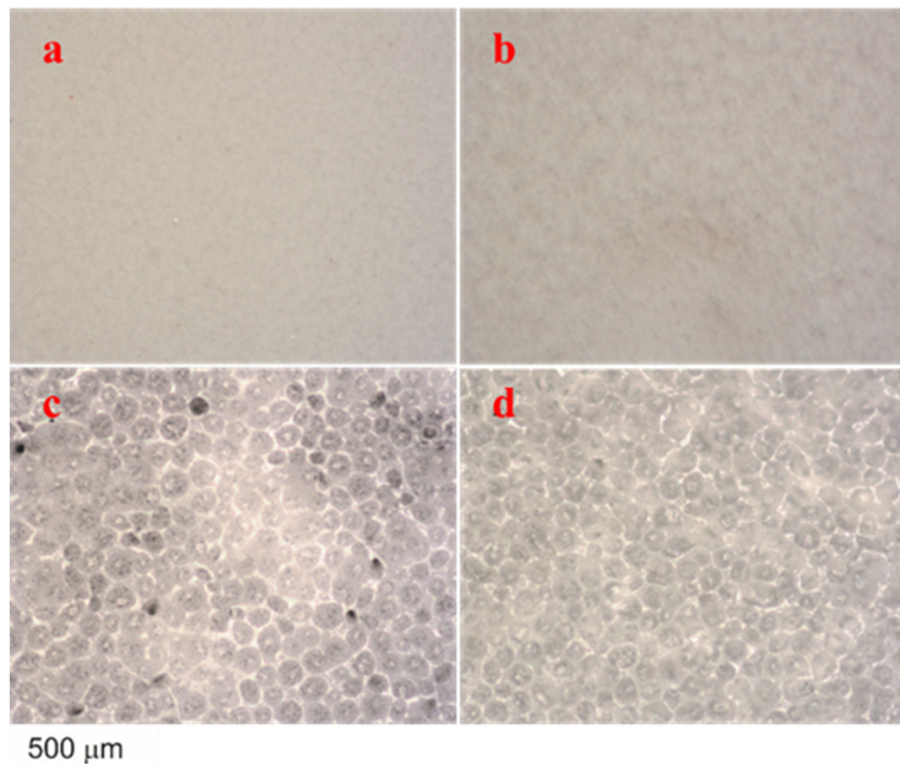


**Figure 4.** Optical microscopy images of the different PCL electrospun membranes and cast films: (a) neat PCL electrospun membranes, (b) PCL/ZnO-NPs electrospun membranes, (c) neat PCL cast film, and (d) PCL/ZnO-NPs cast film.

As an electrospun membrane, the neat electrospun membrane exhibited a quiet, unseen roughness due to its homogeneous smooth surface, whereas the one embedded with ZnO-NPs exhibited a heterogeneous surface with ripples on its surface. Furthermore, the neat PCL cast film exhibited loosely interconnected fissures and pores. As ZnO-NPs were incorporated, these fissures and pores seemed to be reduced and better interconnected.

#### 4.6. Confocal Microscopy (Roughness)

Surface roughness is an important parameter in determining the growth and adhesion of different cell lines for use as biomaterials. The 3D surface plots and profiles of neat electrospun, cast PCL, and their composite membranes and films (PCL/ZnO-NPs) are depicted in Figures 5 and 6.

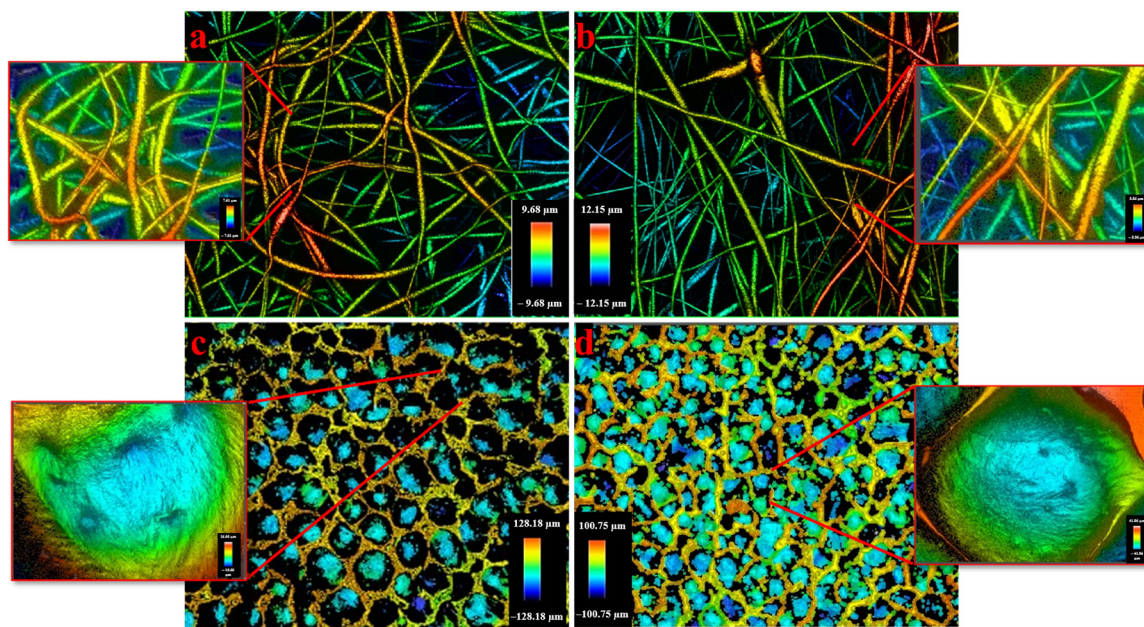


**Figure 5.** The 3D surface plot of the different PCL electrospun membranes and cast films: (a) neat PCL electrospun membranes, (b) PCL/ZnO-NPs electrospun membranes, (c) neat PCL cast film, and (d) PCL/ZnO-NPs cast film.

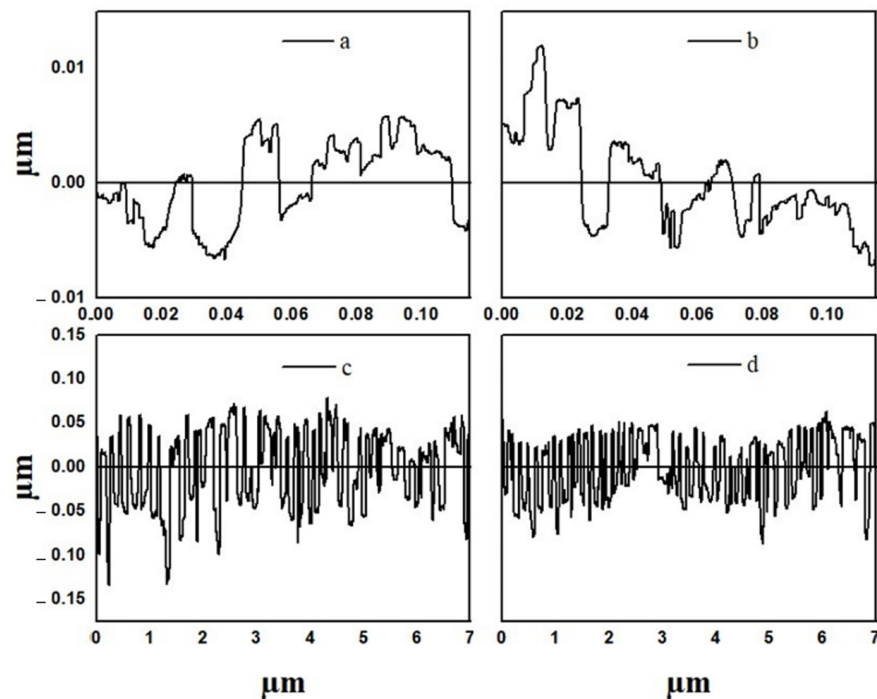


**Figure 6.** Surface profiles of the different PCL electrospun membranes and cast films from selected zones in Figure 5: (a) neat PCL electrospun membranes, (b) PCL/ZnO-NPs electrospun membranes, (c) neat PCL cast film, and (d) PCL/ZnO-NPs cast film.

The roughness analysis was performed at the level of high-resolution images. A summary of the roughness results ( $R_a$  and  $R_q$ ) was included in Table 3.

**Table 3.** Results for nanofiber or pore diameter (nm), roughness average ( $R_a$ ), and root mean square average roughness or quadratic average ( $R_q$ ) of the different PCL electrospun membranes and cast films from selected images in Figure 5.

Sample	Nanofiber or Pore Diameter (nm)	$R_a$ ( $\mu\text{m}$ )		$R_q$ ( $\mu\text{m}$ )	
		All Area	Fiber or Pore	All Area	Fiber or Pore
a	Neat PCL nanofibers	252.5 $\pm$ 4.8 <sup>b</sup>	0.6 <sup>d</sup>	0.6 <sup>d</sup>	0.7 <sup>d</sup>
b	PCL/ZnO-NPs nanofibers	306.4 $\pm$ 5.5 <sup>a</sup>	2.2 <sup>c</sup>	0.9 <sup>c</sup>	2.8 <sup>c</sup>
c	Neat PCL film	244.5 $\pm$ 6.6 <sup>c</sup>	5.4 <sup>b</sup>	2.1 <sup>b</sup>	11.0 <sup>b</sup>
d	PCL/ZnO-NPs film	179.2 $\pm$ 2.7 <sup>d</sup>	13.0 <sup>a</sup>	6.2 <sup>a</sup>	18.8 <sup>a</sup>

Note: Different superscript letters (a–d) of each column indicate heterogeneity of variances ( $p < 0.05$ ).

Therefore, the  $R_a$  and  $R_q$  values (nm) of the cast films were higher than those of the electrospun membrane, most likely due to the fact that the porous and free spaces within the cast films are wider than those within the electrospun membrane, resulting in heterogeneous networks [66]. Nevertheless, when the PCL electrospun membrane and cast film were processed with ZnO-NPs, increases in  $R_a$  and  $R_q$  were observed (Table 3). This is mainly due to the presence of well-dispersed and aggregated nanoparticles. Thus, the surface roughness increases as the average aggregation size increases from two nanoparticles (30 nm) to sixty nanoparticles (888 nm) in different orientations (Section 4.8). Similar altered structures have also been found in other studies [93,94], as confirmed by SEM and TEM analyses.

#### 4.7. Scanning Electron Microscopy (SEM)

An illustration of the morphologies of neat electrospun, cast PCL and their composite membranes and films (PCL/ZnO-NPs) is shown in Figure 7, along with the diameter distributions of the electrospun nanofibers and film pores (summarized in Table 3).

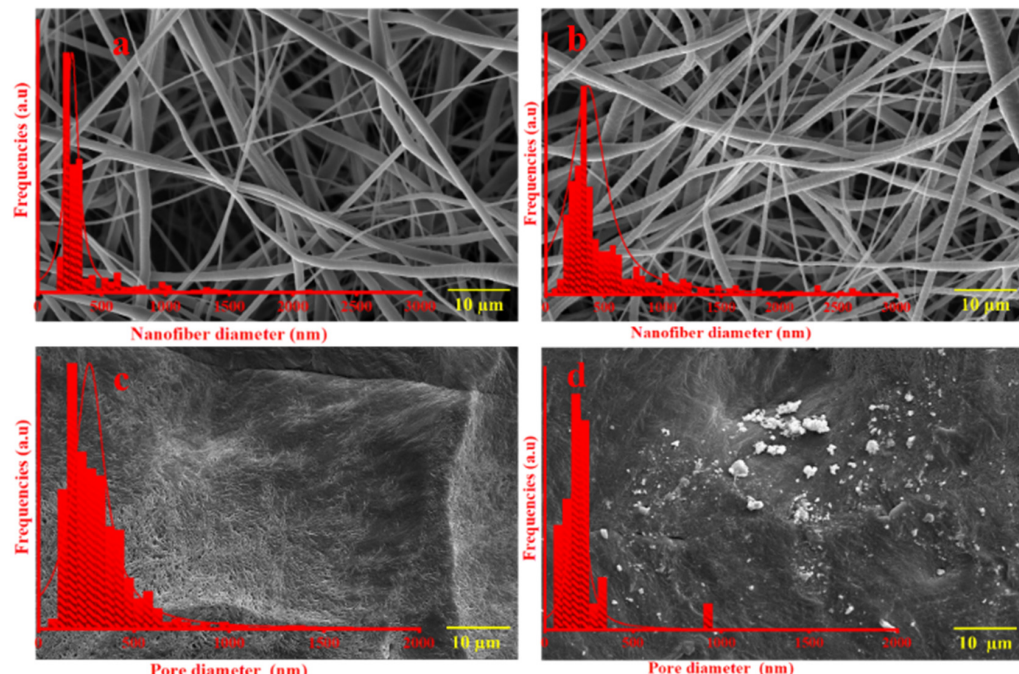


**Figure 7.** Scanning electron microscopy (SEM) images of the different PCL electrospun membranes and cast films: (a) neat PCL electrospun membranes, (b) PCL/ZnO-NPs electrospun membranes, (c) neat PCL cast film, and (d) PCL/ZnO-NPs cast film.

Therefore, the neat PCL membrane exhibits homogeneous, smooth, randomly arranged nanofibers, whereas the neat PCL cast film exhibits a semi-crystalline structure and looks like a multi-layered capillary with fissures and pores.

On the other hand, when ZnO-NPs were incorporated, irregularities and roughness were produced on the nanofiber surface along with an increase in its diameter. Furthermore, the incorporation of ZnO-NPs into the PCL cast films produced roughness and irregularities on the film surface, as well as a reduction in its free pores. This is attributed to the characteristics of nanoparticles during solvent evaporation, including granulation, agglomeration, and dispersion on and within membranes and films [55,71]. The structural characteristics and surface roughness exhibited by nanoparticles were similar to those found in the stands uniformly and the micro-plateaus were sculpted by a solvent evaporation force that lifts them up and wears them down into buttes, mesas, and canyons. However, the aggregation was a little knotty in some places, which may be affected by the concentration of nanoparticles [95]. The findings were similar to those found elsewhere in the literature [96].

#### 4.8. Transmission Electron Microscopy (TEM)

A further illustration of the morphologies of neat electrospun and its composite membranes (PCL/ZnO-NPs) is shown in Figure 8.

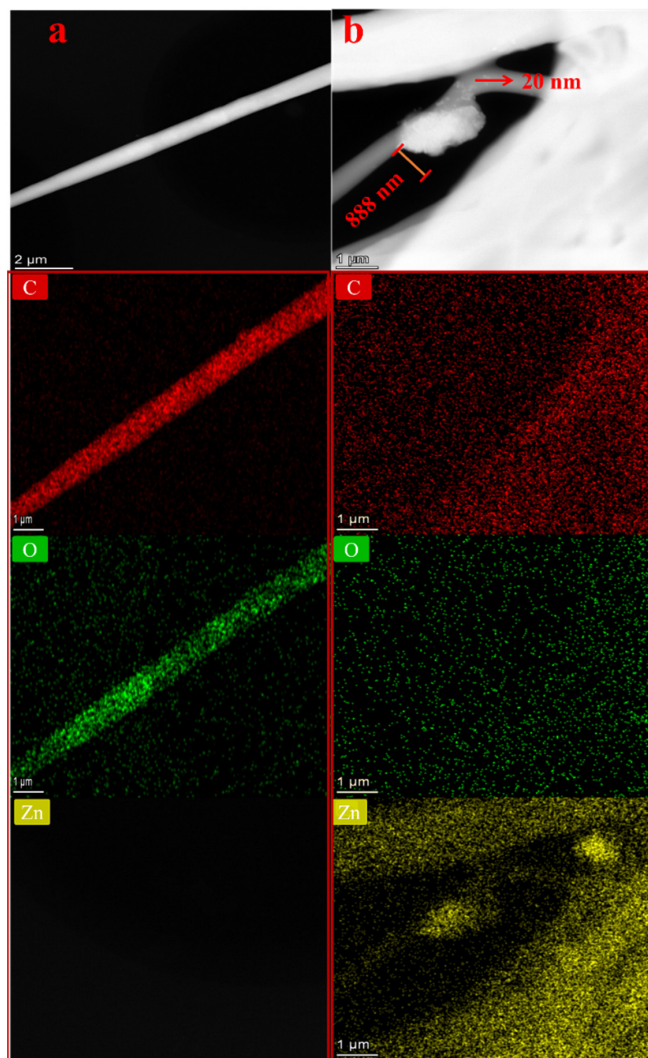


**Figure 8.** Transmission electron microscopy (TEM) images of the different PCL electrospun membranes: (a) neat PCL electrospun membranes, and (b) PCL/ZnO-NPs electrospun membranes.

Furthermore, EDX mappings of the elemental components (Zn, O, and C) were included to confirm the excellent dispersion of ZnO-NPs within the fibers (Figure 8a,b). Accordingly, a uniform distribution of ZnO-NPs was observed, although some aggregation can be observed. As the ZnO-NPs were synthesized using green methods, the aggregation is largely caused by interactions between phytochemical compounds on the ZnO-NP surface and the polymer chains [93,94]. Nanoparticles' aggregation may also be affected by the nature of the solvent; therefore, there may be a variation in the rate at which solvents and non-solvents are interchanged [97]. Regarding this, enhancing the surface roughness of polymer surfaces is essential, since it affects macromolecule adsorption and membrane formation to some extent [98]. The surface roughness measurements were further calculated and are discussed in the next section.

#### 4.9. XRD

The XRD diffractograms of neat electrospun, cast PCL, and composite membranes and films (PCL/ZnO-NPs) are shown in Figure 9, along with the XRD pattern of ZnO-NPs for reference.

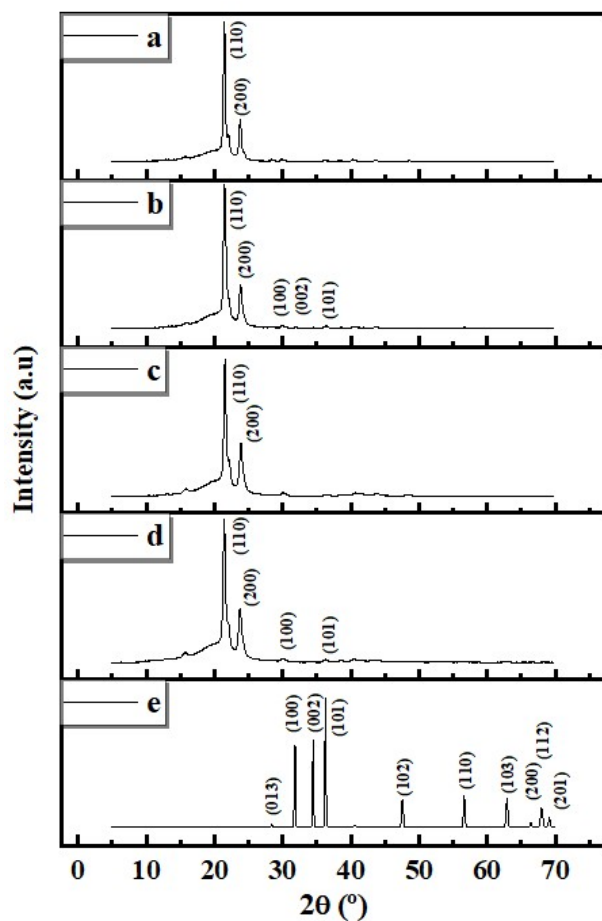


**Figure 9.** XRD spectra of the different PCL electrospun membranes and cast films: (a) neat PCL electrospun membranes, (b) PCL/ZnO-NPs electrospun membranes, (c) neat PCL cast film, (d) PCL/ZnO-NPs cast film, and (e) ZnO-NPs (reference for comparison).

The neat PCL showed peaks near  $21.4^\circ$  and  $24.1^\circ$  corresponding to crystallographic reflection planes (110 and 200, respectively), in agreement with the polymer's crystalline orthorhombic structure. When ZnO-NPs were incorporated, residual peaks corresponding to the ZnO phase were observed (Figure 9b,d). Crystallinity (%) from XRD patterns was determined and is summarized in Table 4.

**Table 4.** XRD results for  $2\theta$  ( $^{\circ}$ ) of the most intense peak (crystallographic plane position corresponding to (110)), full width at the half maximum (FWHM,  $^{\circ}$ ), the distance between the successive, parallel crystallographic planes of atoms (d spacing), and crystallinity degree (crystallinity, %) of the different PCL electrospun membranes and cast films.

	DRX	Pos. (110) ( $^{\circ}$ )	FWHM ( $^{\circ}$ )	d Spacing (110)	Crystallinity (%)
a	Neat PCL nanofibers	21.43	0.311	4.1423	67.4
b	PCL/ZnO-NPs nanofibers	21.49	0.427	4.1325	65.7
c	Neat PCL film	21.53	0.358	4.1233	62.2
d	PCL/ZnO-NPs film	21.42	0.402	4.1455	64.1

As can be observed, values for electrospun mats are slightly higher than those of cast films; thus, crystallization in the direction of the fiber is promoted. However, the effect of ZnO-NPs incorporation is not univocal, thus an increase in crystallinity index (%) was obtained in cast films, whereas it decreased in the electrospun nanofibers. Such variations are subtle and may be assigned to the experimental error, although they have been observed in other systems. For instance, Gibril et al., 2022 [68] incorporated nanocrystalline cellulose and zinc oxide (NCC-ZnO) into PCL-based film (10% w/v in DCM) at different concentrations (2, 4, 6, 8 wt%). They found that the crystallinity degree increased only at 2% (from 59.9 to 61.0%) followed by decreases to 58.7, 52.6, and 42.9% when NCC-ZnO-NPs were incorporated at 4, 6, and 8 wt%, respectively. These decreases in the crystallinity degree were due to the nanofiller aggregation, which confined the mobility of the polymer chains [68].

#### 4.10. DSC

The thermal behavior of neat electrospun cast PCL and composite membranes and films (PCL/ZnO-NPs) was assessed and quantified using DSC curves, as shown in Figure 10.

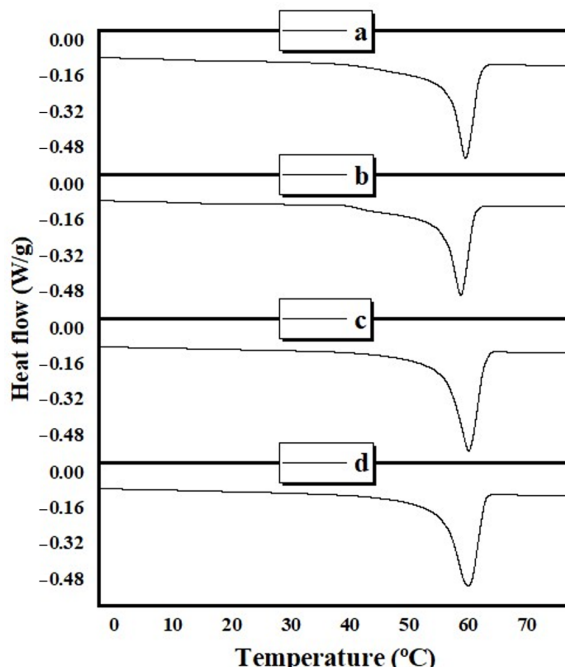


**Figure 10.** DSC thermograms of the different PCL electrospun membranes and cast films: (a) neat PCL electrospun membranes, (b) PCL/ZnO-NPs electrospun membranes, (c) neat PCL cast film, and (d) PCL/ZnO-NPs cast film.

Table 5 summarizes the results for melting temperature ( $T_m$ , °C), fusion enthalpy ( $\Delta H_f$ , J/g), and crystallinity degree ( $\chi_c$ , %).

**Table 5.** DSC results for thermal properties, including melting temperature ( $T_m$ , °C), melting enthalpy ( $\Delta H_f$ , J/g), and crystallization degree ( $\chi_c$ , %) of the different PCL electrospun membranes and cast films.

		$T_m$ (°C)	$\Delta H_f$ (J/g)	$\chi_c$ (%)
a	Neat PCL nanofibers	59.5	69.59	49.9
b	PCL/ZnO-NPs nanofibers	58.7	65.21	46.8
c	Neat PCL film	60.1	75.67	54.2
d	PCL/ZnO-NPs film	60.0	77.99	55.9

Accordingly, the addition of ZnO-NPs (1 wt%) showed a slight decrease in  $T_m$  of the PCL/ZnO-NPs electrospun and cast films, which is probably due to the aggregation of ZnO-NPs with film and membrane chains that hinder the polymer crystallization, forming a thinner lamellar crystal, thereby decreasing the melting temperature [99]. In terms of fusion enthalpy, ZnO-NPs decreased this parameter in the electrospun membrane and increased it in the cast film. Consequently, the crystallinity degree decreased in the presence of ZnO-NPs in the case of PCL/ZnO-NPs electrospun membrane and increased in the cast films. Such an observation was also corroborated by XRD and explained in the previous section by nanoparticle aggregation and the reduction of the mobility of the polymer chains.

The crystallinity degree for PCL reported in the literature was found between 39.1% [62] and 78% [100] (Table 5). Values in this study are around 60%–65%, although there were some differences between the XRD and DSC methods. For instance, according to XRD, the electrospun membranes were more crystalline than the cast films, while the opposite was deduced from DSC. With such a tight range of crystallinity values, it is feasible to reach contradictory conclusions. Both methods have their peculiarities. The XRD is based on a mathematical decomposition into components and the assumption that the peak ratio between amorphous and crystalline phases is quantitative. The DSC is very sensitive to operational conditions (sample weight, instrument calibration, etc.) and to the certainty of the assumption of the melting enthalpy value for a 100% crystalline sample. Consequently, no conclusive results regarding the modification of the crystallinity of samples prepared by either casting or electrospinning can be provided. However, the incorporation of ZnO-NPs had a small effect that was consistently supported by both XRD and DSC. Nevertheless, other studies have concluded that the incorporation of nanoparticles into polymer matrices has no impact on melting or crystallization [61,100]. In this light, it is concluded that the changes in physicochemical and mechanical characteristics, revealed in this study, may be attributed to the incorporation of metal oxide nanoparticles themselves, due to their physicochemical properties.

#### 4.11. Functional Properties (Antioxidant Activity)

The antioxidant activity of neat electrospun and composite membranes (PCL/ZnO-NPs) was assessed by measuring the DPPH• scavenging percentage (SP%) (Figure 11).

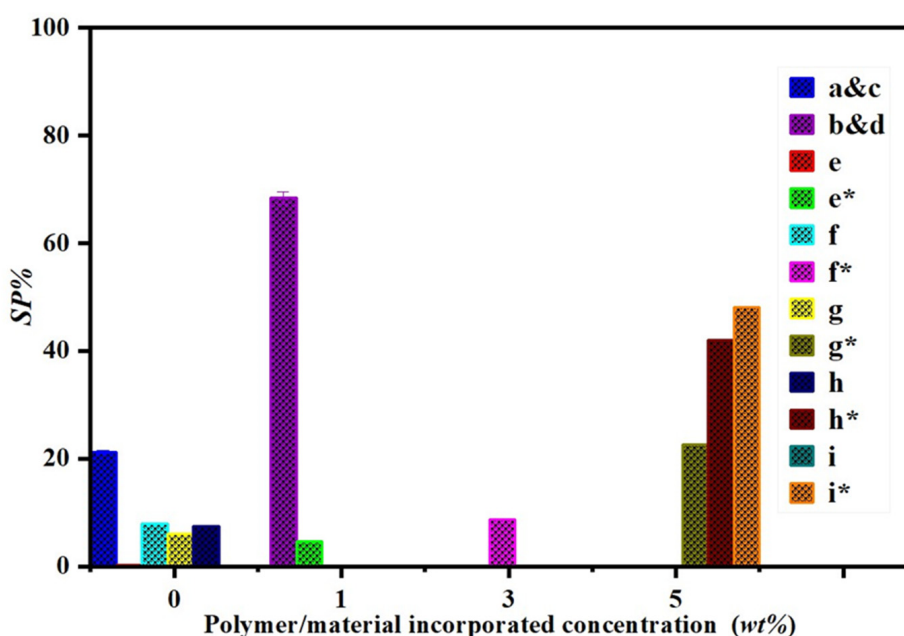


**Figure 11.** DPPH<sup>•</sup> scavenging percentage (SP%) of the different PCL solutions: (a,c) PCL electrospun membranes and film-forming solution without ZnO-NPs included (neat PCL), and (b,d) PCL electrospun membrane and film-forming solution with 1 wt% of ZnO-NPs (PCL/ZnO-NPs). For reference, the literature results are included: e and e\* [101], f and f\* [102], g and g\* [103], h and h\* [104], and i and i\* [105]. (Letters with \* indicate polymer with materials incorporated, and the occulted scale bars e and i indicate zero or negligible antioxidant activity).

A further evaluation was conducted for gallic acid (positive control) with a SP% of 95%. According to Figure 9, the SP% of PCL/ZnO-NPs increased from  $21.2 \pm 0.3$  to  $68.4 \pm 1.2$  (by almost 69% enhancement), demonstrating the beneficial effects of ZnO-NPs on the system in which they are incorporated. This is mainly due to the presence of the phytochemical groups, which produce reactive oxygen species ( $\text{H}_2\text{O}_2$ ,  $\text{O}^{2-}$ ,  ${}^1\text{O}_2$ ,  $-\text{OH}$ ) as antioxidants [54,85,106]. Consequently, the antioxidant property of ZnO-NPs may contribute to their antimicrobial properties, as demonstrated in previous studies [54]. Interestingly, Radisavljevic et al. (2022) have evaluated the DPPH<sup>•</sup> SP% of PCL electrospun (8% w/v in 2,2,2-trifluoroethanol) with the incorporation of yarrow extract at different concentrations (5, 10, 15, and 20 wt%). They found that the SP% increases as the concentration of yarrow extract and incubation time increase, which were about 17, 22, 61 and 55% at 0 h; 48, 75, 90, and 91% after 1 h; and 57, 76, 92, and 92% after 24 h incubation [105]. Another study has reported about 55% of SP% for iron oxide nanoparticles (20% w/w) incorporated into gelatin cast film for 45 min [85]. This study reports about 68% of SP% for 1% wt of ZnO-NPs incubated for 30 min.

## 5. Conclusions

There is increasing interest in the incorporation of nanoparticles of zinc oxide into polycaprolactone-based electrospun membranes and films due to their ability to improve the properties of such membranes and films in a variety of ways. For instance, the reduction of water vapor permeability and the increment of surface hydrophobicity adds potential uses. Furthermore, the incorporation of ZnO-NPs increased the opacity of both the membrane and the film by blocking light transmission. In addition, the PCL containing ZnO-NPs provided superior mechanical performance and antioxidant activity than the PCL without ZnO-NPs. A significant effect of ZnO-NPs was the increase in the roughness of polymer surfaces, which facilitates macromolecule adsorption. However, nanoparticles may show some contradictory behaviors in terms of melting temperatures and crystallizations, as they tend to agglomerate or aggregate, and thus they do not have a significant effect on these properties.

Moreover, this study shows that green ZnO-NPs possess numerous beneficial properties, including a substantial increase in antioxidant activity. Furthermore, zinc oxide nanoparticles will benefit future applications, such as eliminating toxic waste and reducing costs. A well-controlled dispersion of green ZnO-NPs in both electrospun nanofibrous membranes and cast films may enhance their functional properties in sustainable applications. The combination of all the characteristics discussed above makes PCL suitable for a variety of applications, including pharmaceutical biomaterials, therapeutic applications, and agricultural uses.

**Author Contributions:** Conceptualization, J.A.A.A., A.R. and A.G.; methodology, J.A.A.A. and A.R.; software, J.A.A.A. and J.J.B.; validation, J.A.A.A. and A.R.; formal analysis, J.A.A.A.; investigation, J.A.A.A., J.J.B. and A.R.; resources, J.J.B. and A.G.; data curation, J.A.A.A.; writing—original draft preparation, J.A.A.A. and J.J.B.; writing—review and editing, A.G. and A.R.; visualization, A.G. and A.R.; supervision, J.J.B. and A.R.; project administration, A.G.; funding acquisition, A.R. All authors have read and agreed to the published version of the manuscript.

**Funding:** This study was financially supported by MCIN/AEI/10.13039/501100011033/FEDER, UE, a way to make Europe through the project PID2021-124294OB-C21.

**Institutional Review Board Statement:** Not applicable.

**Informed Consent Statement:** Not applicable.

**Data Availability Statement:** The data presented in this study are available on request from the corresponding author.

**Acknowledgments:** The authors acknowledge the MCI/AEI/FEDER, EU project (Ref. PID2021-124294OB-C21) that supported this work. In addition, the authors are grateful for the predoctoral grant from J.A.A.A. (Universidad de Sevilla, CODE 810). J.A.A.A. also would like to thank the support from HSA Group represented by Abdul Jabbar Hayel Saeed Anam. The authors also thank CITIUS for granting access to and their assistance with the SEM and TEM area characterization, and microscopy services. The authors would like to extend special thanks to Consuelo Cerrillos for helping with 3D optical profiling.

**Conflicts of Interest:** The authors declare no conflict of interest.

## References

1. Nayak, R.; Padhye, R.; Arnold, L. Melt-electrospinning of nanofibers. In *Electrospun Nanofibers*; Elsevier: Amsterdam, The Netherlands, 2017; pp. 11–40.
2. Yew, C.H.T.; Azari, P.; Choi, J.R.; Muhamad, F.; Pingguan-Murphy, B. Electrospun polycaprolactone nanofibers as a reaction membrane for lateral flow assay. *Polymers* **2018**, *10*, 1387. [[CrossRef](#)]
3. Rathore, P.; Schiffman, J.D. Beyond the Single-Nozzle: Coaxial Electrospinning Enables Innovative Nanofiber Chemistries, Geometries, and Applications. *ACS Appl. Mater. Interfaces* **2021**, *13*, 48–66. [[CrossRef](#)]
4. Chinnappan, B.A.; Krishnaswamy, M.; Xu, H.; Hoque, M.E. Electrospinning of Biomedical Nanofibers/Nanomembranes: Effects of Process Parameters. *Polymers* **2022**, *14*, 3719. [[CrossRef](#)]
5. Mamun, A.; Sabantina, L.; Klöcker, M.; Heide, A.; Blachowicz, T.; Ehrmann, A. Electrospinning Nanofiber Mats with Magnetite Nanoparticles Using Various Needle-Based Techniques. *Polymers* **2022**, *14*, 533. [[CrossRef](#)] [[PubMed](#)]
6. Lee, D.Y.; Lee, K.H.; Kim, B.Y.; Cho, N.I. Silver nanoparticles dispersed in electrospun polyacrylonitrile nanofibers via chemical reduction. *J. Sol.-Gel. Sci. Technol.* **2010**, *54*, 63–68. [[CrossRef](#)]
7. Greiner, A.; Wendorff, J.H. Electrospinning: A fascinating method for the preparation of ultrathin fibers. *Angew. Chem. Int. Ed.* **2007**, *46*, 5670–5703. [[CrossRef](#)] [[PubMed](#)]
8. Klinkhammer, K.; Seiler, N.; Grafahrend, D.; Gerardo-Navia, J.; Mey, J.; Brook, G.A.; Möller, M.; Dalton, P.D.; Klee, D. Deposition of Electrospun Fibers on Reactive Substrates for In Vitro Investigations. *Tissue Eng. Part C Methods* **2009**, *15*, 77–85. [[CrossRef](#)]
9. Grothe, T.; Wehlage, D.; Böhm, T.; Remche, A.; Ehrmann, A. Brezigelno elektropredenje PAN novovlaknatih kopren. *Tekstilec* **2017**, *60*, 290–295. [[CrossRef](#)]
10. García-Mateos, F.J.; Cordero-Lanzac, T.; Berenguer, R.; Morallón, E.; Cazorla-Amorós, D.; Rodríguez-Mirasol, J.; Cordero, T. Lignin-derived Pt supported carbon (submicron)fiber electrocatalysts for alcohol electro-oxidation. *Appl. Catal. B Environ.* **2017**, *211*, 18–30. [[CrossRef](#)]
11. Che Othman, F.E.; Yusof, N.; Hasbullah, H.; Jaafar, J.; Ismail, A.F.; Abdullah, N.; Md Nordin, N.A.H.; Aziz, F.; Wan Salleh, W.N. Polyacrylonitrile/magnesium oxide-based activated carbon nanofibers with well-developed microporous structure and their adsorption performance for methane. *J. Ind. Eng. Chem.* **2017**, *51*, 281–287. [[CrossRef](#)]

12. Prabu, G.T.V.; Dhurai, B. A Novel Profiled Multi-Pin Electrospinning System for Nanofiber Production and Encapsulation of Nanoparticles into Nanofibers. *Sci. Rep.* **2020**, *10*, 4302. [CrossRef] [PubMed]
13. Gao, S.; Tang, G.; Hua, D.; Xiong, R.; Han, J.; Jiang, S.; Zhang, Q.; Huang, C. Stimuli-responsive bio-based polymeric systems and their applications. *J. Mater. Chem. B* **2019**, *7*, 709–729. [CrossRef] [PubMed]
14. Mamun, A. Review of possible applications of nanofibrous mats for wound dressings. *Tekstilec* **2019**, *62*, 89–100. [CrossRef]
15. Wehlage, D.; Blattner, H.; Mamun, A.; Kutzli, I.; Diestelhorst, E.; Rattenholl, A.; Gudermann, F.; Lütkemeyer, D.; Ehrmann, A. Cell growth on electrospun nanofiber mats from polyacrylonitrile (PAN) blends. *AIMS Bioeng.* **2020**, *7*, 43–54. [CrossRef]
16. Boyraz, E.; Yalcinkaya, F.; Hruza, J.; Maryska, J. Surface-modified nanofibrous PVDF membranes for liquid separation technology. *Materials* **2019**, *12*, 2702. [CrossRef]
17. Kozior, T.; Trabelsi, M.; Mamun, A.; Sabantina, L.; Ehrmann, A. Stabilization of Electrospun Nanofiber Mats Used for Filters by 3D Printing. *Polymers* **2019**, *11*, 1618. [CrossRef]
18. Yalcinkaya, F.; Boyraz, E.; Maryska, J.; Kucerova, K. A review on membrane technology and chemical surface modification for the oily wastewater treatment. *Materials* **2020**, *13*, 493. [CrossRef]
19. Xue, Y.; Guo, X.; Zhou, H.; Zhou, J. Influence of beads-on-string on Na-Ion storage behaviors of electrospun carbon nanofibers. *Carbon N. Y.* **2019**, *154*, 219–229. [CrossRef]
20. Kohn, S.; Wehlage, D.; Junger, I.J.; Ehrmann, A. Electrospinning a dye-sensitized solar cell. *Catalysts* **2019**, *9*, 975. [CrossRef]
21. Li, X.; Chen, W.; Qian, Q.; Huang, H.; Chen, Y.; Wang, Z.; Chen, Q.; Yang, J.; Li, J.; Mai, Y.W. Electrospinning-Based Strategies for Battery Materials. *Adv. Energy Mater.* **2021**, *11*, 2000845. [CrossRef]
22. Abutaleb, A. Catalytic and photocatalytic electrospun nanofibers for hydrogen generation from ammonia borane complex: A review. *Polymers* **2021**, *13*, 2290. [CrossRef] [PubMed]
23. Gangemi, C.M.A.; Iudici, M.; Spitaleri, L.; Randazzo, R.; Gaeta, M.; D’Urso, A.; Gulino, A.; Purrello, R.; Fragalà, M.E. Polyether-sulfone Mats Functionalized with Porphyrin for Removal of Para-nitroaniline from Aqueous Solution. *Molecules* **2019**, *24*, 3344. [CrossRef] [PubMed]
24. Contreras-Cáceres, R.; Cabeza, L.; Perazzoli, G.; Díaz, A.; López-Romero, J.M.; Melguizo, C.; Prados, J. Electrospun nanofibers: Recent applications in drug delivery and cancer therapy. *Nanomaterials* **2019**, *9*, 656. [CrossRef]
25. Salmeri, M.; Ognibene, G.; Saitta, L.; Lombardo, C.; Genovese, C.; Barcellona, M.; D’Urso, A.; Spitaleri, L.; Blanco, I.; Cicala, G.; et al. Optimization of ZnO nanorods growth on polyetheresulfone electrospun mats to promote antibacterial properties. *Molecules* **2020**, *25*, 1696. [CrossRef]
26. Wang, F.; Xie, Z.; Liang, J.; Fang, B.; Piao, Y.; Hao, M.; Wang, Z. Tourmaline-Modified FeMnTiO<sub>x</sub> Catalysts for Improved Low-Temperature NH<sub>3</sub>-SCR Performance. *Environ. Sci. Technol.* **2019**, *53*, 6989–6996. [CrossRef]
27. Ouyang, J.; Zhao, Z.; Yang, H.; Zhang, Y.; Tang, A. Large-scale synthesis of sub-micro sized halloysite-composed CZA with enhanced catalysis performances. *Appl. Clay Sci.* **2018**, *152*, 221–229. [CrossRef]
28. Piao, Y.; Jiang, Q.; Li, H.; Matsumoto, H.; Liang, J.; Liu, W.; Pham-Huu, C.; Liu, Y.; Wang, F.; Liu, W.; et al. Identify Zr Promotion Effects in Atomic Scale for Co-Based Catalysts in Fischer-Tropsch Synthesis. *ACS Catal.* **2020**, *10*, 7894–7906. [CrossRef]
29. Tian, J.; Deng, H.; Huang, M.; Liu, R.; Yi, Y.; Dong, X. Electrospun Nanofibers for Food and Food Packaging Technology. In *Electrospinning: Nanofabrication and Applications*; Elsevier: Amsterdam, The Netherlands, 2019; pp. 455–516.
30. Menkhaus, T.J.; Fong, H. Electrospun Nanofibers for Protein Adsorption. In *Electrospinning: Nanofabrication and Applications*; Elsevier: Amsterdam, The Netherlands, 2019; pp. 517–542.
31. Sheng, J.; Zhao, J.; Yu, X.; Liu, L.; Yu, J.; Ding, B. Electrospun Nanofibers for Waterproof and Breathable Clothing. In *Electrospinning: Nanofabrication and Applications*; Elsevier: Amsterdam, The Netherlands, 2019; pp. 543–570.
32. Li, Y.; Abedalwafa, M.A.; Tang, L.; Li, D.; Wang, L. Electrospun Nanofibers for Sensors. In *Electrospinning: Nanofabrication and Applications*; Elsevier: Amsterdam, The Netherlands, 2019; pp. 571–601.
33. Hu, J.; Zhang, K.-Q. Electrospun Nanofibers for Optical Applications. In *Electrospinning: Nanofabrication and Applications*; Elsevier: Amsterdam, The Netherlands, 2019; pp. 603–617.
34. Zhai, Y.; Liu, H.; Li, L.; Yu, J.; Ding, B. Electrospun Nanofibers for Lithium-Ion Batteries. In *Electrospinning: Nanofabrication and Applications*; Elsevier: Amsterdam, The Netherlands, 2019; pp. 671–694.
35. Duque Sánchez, L.; Brack, N.; Postma, A.; Pigram, P.J.; Meagher, L. Surface modification of electrospun fibres for biomedical applications: A focus on radical polymerization methods. *Biomaterials* **2016**, *106*, 24–45. [CrossRef]
36. Mao, W.; Yoo, H.S. Pluronic-Induced Surface Etching of Biodegradable Nanofibers for Enhanced Adsorption of Serum Protein. *Macromol. Biosci.* **2017**, *17*, 1700057. [CrossRef]
37. Shahmoradi, S.; Yazdian, F.; Tabandeh, F.; Soheili, Z.-S.; Hatamian Zarami, A.S.; Navaei-Nigjeh, M. Controlled surface morphology and hydrophilicity of polycaprolactone toward human retinal pigment epithelium cells. *Mater. Sci. Eng. C* **2017**, *73*, 300–309. [CrossRef]
38. Perez-Puyana, V.; Wieringa, P.; Guerrero, A.; Romero, A.; Moroni, L. (Macro)Molecular Imprinting of Proteins on PCL Electrospun Scaffolds. *ACS Appl. Mater. Interfaces* **2021**, *13*, 29293–29302. [CrossRef] [PubMed]
39. Nwakaudu, A.A.; Nwakaudu, M.S.; Owuamanam, C.I.; Iheaturu, N.C. The Use of Natural Antioxidant Active Polymer Packaging Films for Food Preservation. *Appl. Signals Rep.* **2015**, *2*, 38–50.
40. Wang, Y.; Yang, Q.; Shan, G.; Wang, C.; Du, J.; Wang, S.; Li, Y.; Chen, X.; Jing, X.; Wei, Y. Preparation of silver nanoparticles dispersed in polyacrylonitrile nanofiber film spun by electrospinning. *Mater. Lett.* **2005**, *59*, 3046–3049. [CrossRef]

41. Kizildag, N. Nanocomposite Nanofibers of Polyacrylonitrile (PAN) and Silver Nanoparticles (AgNPs) Electrospun from Dimethylsulfoxide. *Marmara Univ. J. Sci.* **2015**, *27*, 15–18. [CrossRef]
42. Kumar, M.; Isloor, A.M.; Somasekhara Rao, T.; Ismail, A.F.; Farnood, R.; Nambissan, P.M.G. Removal of toxic arsenic from aqueous media using polyphenylsulfone/cellulose acetate hollow fiber membranes containing zirconium oxide. *Chem. Eng. J.* **2020**, *393*, 124367. [CrossRef]
43. Myronchuk, V.; Dzyazko, Y.; Ukrainets, A.; Bildukovich, A.; Kornienko, L.; Rozhdestvenskaya, L.; Palchik, A. Organic-inorganic membranes for filtration of corn distillery. *Acta Period. Technol.* **2016**, *47*, 153–165. [CrossRef]
44. Agrawal, A.; Sharma, A.; Awasthi, K.K.; Awasthi, A. Metal oxides nanocomposite membrane for biofouling mitigation in wastewater treatment. *Mater. Today Chem.* **2021**, *21*, 100532. [CrossRef]
45. Mallakpour, S.; Nouruzi, N. Effect of modified ZnO nanoparticles with biosafe molecule on the morphology and physiochemical properties of novel polycaprolactone nanocomposites. *Polymer* **2016**, *89*, 94–101. [CrossRef]
46. Augustine, R.; Malik, H.N.; Singhal, D.K.; Mukherjee, A.; Malakar, D.; Kalarikkal, N.; Thomas, S. Electrospun polycaprolactone/ZnO nanocomposite membranes as biomaterials with antibacterial and cell adhesion properties. *J. Polym. Res.* **2014**, *21*, 347. [CrossRef]
47. Tran, N.; Mir, A.; Mallik, D.; Sinha, A.; Nayar, S.; Webster, T.J. Bactericidal effect of iron oxide nanoparticles on *Staphylococcus aureus*. *Int. J. Nanomed.* **2010**, *5*, 277–283. [CrossRef]
48. Zhang, Z.; Han, M. One-step preparation of size-selected and well-dispersed silver nanocrystals in polyacrylonitrile by simultaneous reduction and polymerization. *J. Mater. Chem.* **2003**, *13*, 641–643. [CrossRef]
49. Lee, D.-Y.; Cho, J.-E.; Kim, Y.-N.; Oh, Y.-J. Gas sensing properties of polyacrylonitrile/metal oxide nanofibrous mat prepared by electrospinning. *J. Sens. Sci. Technol.* **2008**, *17*, 281–288. [CrossRef]
50. Pastoriza-Santos, I.; Serra-Rodríguez, C.; Liz-Marzáñ, L.M. Self-assembly of silver particle monolayers on glass from Ag<sup>+</sup> solutions in DMF. *J. Colloid Interface Sci.* **2000**, *221*, 236–241. [CrossRef] [PubMed]
51. Abdullah, J.A.A.; Jiménez-Rosado, M.; Guerrero, A.; Romero, A. Biopolymer-Based Films Reinforced with Green Synthesized Zinc Oxide Nanoparticles. *Polymers* **2022**, *14*, 5202. [CrossRef]
52. Abdullah, J.A.A.; Jiménez-Rosado, M.; Benítez, J.J.; Guerrero, A.; Romero, A. Biopolymer-Based Films Reinforced with Fe<sub>x</sub>O<sub>y</sub>-Nanoparticles. *Polymers* **2022**, *14*, 4487. [CrossRef]
53. ASTM E96/E96M-10; Standard Test Methods for Water Vapor Transmission of Materials. ASTM International: West Conshohocken, PA, USA, 2010. [CrossRef]
54. Abdullah, J.A.A.; Jiménez-Rosado, M.; Guerrero, A.; Romero, A. Gelatin-Based Biofilms with Fe<sub>x</sub>O<sub>y</sub>-NPs Incorporated for Antioxidant and Antimicrobial Applications. *Materials* **2022**, *15*, 1966. [CrossRef]
55. Soltanzadeh, M.; Peighambardoust, S.H.; Ghanbarzadeh, B.; Amjadi, S.; Mohammadi, M.; Lorenzo, J.M.; Hamishehkar, H. Active gelatin/cress seed gum-based films reinforced with chitosan nanoparticles encapsulating pomegranate peel extract: Preparation and characterization. *Food Hydrocoll.* **2022**, *129*, 107620. [CrossRef]
56. UNE-EN ISO 527-3: Plásticos. Determinación de las Propiedades en Tracción. Parte 3: Condiciones de Ensayo para Películas y Hojas. AENOR: Madrid, Spain, 2019.
57. El, S.; Koraichi, S.; Latrache, H.; Hamadi, F. Scanning Electron Microscopy (SEM) and Environmental SEM: Suitable Tools for Study of Adhesion Stage and Biofilm Formation. In *Scanning Electron Microscopy*; InTech: London, UK, 2012.
58. ISO 4287:1997; Geometrical Product Specifications (GPS)—Surface Texture: Profile Method—Terms, Definitions and Surface Texture Parameters—Amendment 1: Peak Count Number. ISO: Genève, Switzerland, 2009.
59. Barzinjy, A.A.; Azeez, H.H. Green synthesis and characterization of zinc oxide nanoparticles using *Eucalyptus globulus* Labill. leaf extract and zinc nitrate hexahydrate salt. *SN Appl. Sci.* **2020**, *2*, 991. [CrossRef]
60. Borghesi, D.C.; Molina, M.F.; Guerra, M.A.; Campos, M.G.N. Biodegradation study of a novel poly-caprolactone-coffee husk composite film. *Mater. Res.* **2016**, *19*, 752–758. [CrossRef]
61. Fukushima, K.; Tabuani, D.; Camino, G. Nanocomposites of PLA and PCL based on montmorillonite and sepiolite. *Mater. Sci. Eng. C* **2009**, *29*, 1433–1441. [CrossRef]
62. Elen, K.; Murariu, M.; Peeters, R.; Dubois, P.; Mullens, J.; Hardy, A.; Van Bael, M.K. Towards high-performance biopackaging: Barrier and mechanical properties of dual-action polycaprolactone/zinc oxide nanocomposites. *Polym. Adv. Technol.* **2012**, *23*, 1422–1428. [CrossRef]
63. L’Abee, R.; Van Duin, M.; Goossens, H. Crystallization kinetics and crystalline morphology of poly( $\epsilon$ -caprolactone) in blends with grafted rubber particles. *J. Polym. Sci. Part B Polym. Phys.* **2010**, *48*, 1438–1448. [CrossRef]
64. Blázquez-Blázquez, E.; Pérez, E.; Lorenzo, V.; Cerrada, M.L. Crystalline Characteristics and Their Influence in the High Density Polyethylene Blends. *Polymers* **2019**, *11*, 1874. [CrossRef] [PubMed]
65. Li, T.; Wang, Y.; Wang, X.; Cheng, C.; Zhang, K.; Yang, J.; Han, G.; Wang, Z.; Wang, X.; Wang, L. Desalination Characteristics of Cellulose Acetate FO Membrane Incorporated with ZIF-8 Nanoparticles. *Membranes* **2022**, *12*, 122. [CrossRef] [PubMed]
66. Guarino, V.; Alvarez-perez, M.; Cirillo, V.; Ambrosio, L. hMSC interaction with PCL and PCL/gelatin platforms: A comparative study on films and electrospun membranes. *J. Bioact. Compat. Polym.* **2011**, *26*, 144–160. [CrossRef]
67. Stafiej, P.; Küng, F.; Kruse, F.E.; Schubert, D.W.; Fuchsluger, T.A. Mechanical and Optical Properties of PCL Nanofiber Reinforced Alginate Hydrogels for Application in Corneal Wound Healing. *Biomater. Med. Appl. Res.* **2018**, *2*, 1–9. [CrossRef]

68. Gibril, M.E.; Ahmed, K.K.; Lekha, P.; Sithole, B.; Khosla, A.; Furukawa, H. Effect of nanocrystalline cellulose and zinc oxide hybrid organic–inorganic nanofiller on the physical properties of polycaprolactone nanocomposite films. *Microsyst. Technol.* **2022**, *28*, 143–152. [[CrossRef](#)]
69. Ni, S.; Zhang, H.; Godwin, P.M.; Dai, H.; Xiao, H. ZnO nanoparticles enhanced hydrophobicity for starch film and paper. *Mater. Lett.* **2018**, *230*, 207–210. [[CrossRef](#)]
70. Wongphan, P.; Panrong, T.; Harnkarnsujarit, N. Effect of different modified starches on physical, morphological, thermomechanical, barrier and biodegradation properties of cassava starch and polybutylene adipate terephthalate blend film. *Food Packag. Shelf Life* **2022**, *32*, 100844. [[CrossRef](#)]
71. Drobota, M.; Vlad, S.; Gradinaru, L.M.; Bargan, A.; Radu, I.; Butnaru, M.; Rîmbu, C.M.; Ciobanu, R.C.; Aflori, M. Composite Materials Based on Gelatin and Iron Oxide Nanoparticles for MRI Accuracy. *Materials* **2022**, *15*, 3479. [[CrossRef](#)]
72. Mosleh, Y.; de Zeeuw, W.; Nijemeisland, M.; Bijleveld, J.C.; van Duin, P.; Pouli, J.A. The Structure–Property Correlations in Dry Gelatin Adhesive Films. *Adv. Eng. Mater.* **2021**, *23*, 2000716. [[CrossRef](#)]
73. Chen, K.; Yu, J.; Huang, J.; Tang, Q.; Li, H.; Zou, Z. Improved mechanical, water vapor barrier and UV-shielding properties of cellulose acetate films with flower-like metal-organic framework nanoparticles. *Int. J. Biol. Macromol.* **2021**, *167*, 1–9. [[CrossRef](#)]
74. Zhou, H.; Tong, H.; Lu, J.; Cheng, Y.; Qian, F.; Tao, Y.; Wang, H. Preparation of bio-based cellulose acetate/chitosan composite film with oxygen and water resistant properties. *Carbohydr. Polym.* **2021**, *270*, 118381. [[CrossRef](#)] [[PubMed](#)]
75. Rhim, J.W.; Hong, S.I.; Park, H.M.; Ng, P.K.W. Preparation and characterization of chitosan-based nanocomposite films with antimicrobial activity. *J. Agric. Food Chem.* **2006**, *54*, 5814–5822. [[CrossRef](#)] [[PubMed](#)]
76. Ghosal, K.; Chandra, A.; Praveen, G.; Snigdha, S.; Roy, S.; Agatemor, C.; Thomas, S.; Provaznik, I. Electrospinning over Solvent Casting: Tuning of Mechanical Properties of Membranes. *Sci. Rep.* **2018**, *8*, 5058. [[CrossRef](#)]
77. De Moura, M.R.; Aouada, F.A.; Avena-Bustillos, R.J.; McHugh, T.H.; Krochta, J.M.; Mattoso, L.H.C. Improved barrier and mechanical properties of novel hydroxypropyl methylcellulose edible films with chitosan/tripolyphosphate nanoparticles. *J. Food Eng.* **2009**, *92*, 448–453. [[CrossRef](#)]
78. Hosseini, S.F.; Rezaei, M.; Zandi, M.; Farahmandghavi, F. Fabrication of bio-nanocomposite films based on fish gelatin reinforced with chitosan nanoparticles. *Food Hydrocoll.* **2015**, *44*, 172–182. [[CrossRef](#)]
79. Vanin, F.M.; Hirano, M.H.; Carvalho, R.A.; Moraes, I.C.F.; Bittante, A.M.Q.B.; Sobral, P.J.d.A. Development of active gelatin-based nanocomposite films produced in an automatic spreader. *Food Res. Int.* **2014**, *63*, 16–24. [[CrossRef](#)]
80. Martucci, J.F.; Ruseckaite, R.A. Antibacterial activity of gelatin/copper (II)-exchanged montmorillonite films. *Food Hydrocoll.* **2017**, *64*, 70–77. [[CrossRef](#)]
81. Benito-González, I.; López-Rubio, A.; Martínez-Sanz, M. Potential of lignocellulosic fractions from *Posidonia oceanica* to improve barrier and mechanical properties of bio-based packaging materials. *Int. J. Biol. Macromol.* **2018**, *118*, 542–551. [[CrossRef](#)]
82. Rodrigues, M.Á.V.; Bertolo, M.R.V.; Marangon, C.A.; Martins, V.d.C.A.; Plepis, A.M.d.G. Chitosan and gelatin materials incorporated with phenolic extracts of grape seed and jabuticaba peel: Rheological, physicochemical, antioxidant, antimicrobial and barrier properties. *Int. J. Biol. Macromol.* **2020**, *160*, 769–779. [[CrossRef](#)]
83. Shankar, S.; Wang, L.-F.; Rhim, J. Effect of melanin nanoparticles on the mechanical, water vapor barrier, and antioxidant properties of gelatin-based films for food packaging application. *Food Packag. Shelf Life* **2019**, *21*, 100363. [[CrossRef](#)]
84. Spatafora Salazar, A.S.; Sáenz Cavazos, P.A.; Mujica Paz, H.; Valdez Fragoso, A. External factors and nanoparticles effect on water vapor permeability of pectin-based films. *J. Food Eng.* **2019**, *245*, 73–79. [[CrossRef](#)]
85. Mehmood, Z.; Sadiq, M.B.; Khan, M.R. Gelatin nanocomposite films incorporated with magnetic iron oxide nanoparticles for shelf life extension of grapes. *J. Food Saf.* **2020**, *40*, e12814. [[CrossRef](#)]
86. Kanmani, P.; Rhim, J.W. Physicochemical properties of gelatin/silver nanoparticle antimicrobial composite films. *Food Chem.* **2014**, *148*, 162–169. [[CrossRef](#)] [[PubMed](#)]
87. Šupová, M.; Martynková, G.S.; Barabaszová, K. Effect of nanofillers dispersion in polymer matrices: A review. *Sci. Adv. Mater.* **2011**, *3*, 1–25. [[CrossRef](#)]
88. Chatkitanan, T.; Harnkarnsujarit, N. Effects of nitrite incorporated active films on quality of pork. *Meat Sci.* **2021**, *172*, 108367. [[CrossRef](#)]
89. Yadav, M. Study on thermal and mechanical properties of cellulose/iron oxide bionanocomposites film. *Compos. Commun.* **2018**, *10*, 1–5. [[CrossRef](#)]
90. Leelaphiwat, P.; Pechprakan, C.; Siriphop, P.; Bumbudsanpharoke, N.; Harnkarnsujarit, N. Effects of nisin and EDTA on morphology and properties of thermoplastic starch and PBAT biodegradable films for meat packaging. *Food Chem.* **2022**, *369*, 130956. [[CrossRef](#)]
91. Klinmalai, P.; Srisa, A.; Laorenza, Y.; Katekhong, W. Antifungal and plasticization effects of carvacrol in biodegradable poly (lactic acid) and poly (butylene adipate terephthalate) blend films for bakery packaging. *LWT* **2021**, *152*, 112356. [[CrossRef](#)]
92. An, L.; Zhang, D.; Zhang, L.; Feng, G. Effect of nanoparticle size on the mechanical properties of nanoparticle assemblies. *Nanoscale* **2019**, *11*, 9563–9573. [[CrossRef](#)] [[PubMed](#)]
93. Villasante, J.; Martin-Lujano, A.; Almajano, M.P. Characterization and application of gelatin films with pecan walnut and shell extract (*Carya illinoiensis*). *Polymers* **2020**, *12*, 1424. [[CrossRef](#)] [[PubMed](#)]

94. Phothisarattana, D.; Wongphan, P.; Promhuad, K.; Promsorn, J.; Harnkarnsujarit, N. Biodegradable Poly(Butylene Adipate-Co-Terephthalate) and Thermoplastic Starch-Blended TiO<sub>2</sub> Nanocomposite Blown Films as Functional Active Packaging of Fresh Fruit. *Polymers* **2021**, *13*, 4192. [[CrossRef](#)]
95. Phothisarattana, D.; Harnkarnsujarit, N. Migration, aggregations and thermal degradation behaviors of TiO<sub>2</sub> and ZnO incorporated PBAT/TPS nanocomposite blown films. *Food Packag. Shelf Life* **2022**, *33*, 100901. [[CrossRef](#)]
96. Ghasemi-Mobarakeh, L.; Prabhakaran, M.P.; Morshed, M.; Nasr-Esfahani, M.H.; Ramakrishna, S. Electrospun poly( $\epsilon$ -caprolactone)/gelatin nanofibrous scaffolds for nerve tissue engineering. *Biomaterials* **2008**, *29*, 4532–4539. [[CrossRef](#)]
97. Boughdiri, A.; Ounifi, I.; Chemingui, H.; Ursino, C.; Gordano, A.; Zouaghi, M.O.; Hafiane, A.; Figoli, A.; Ferjani, E. A preliminary study on cellulose acetate composite membranes: Effect of nanoparticles types in their preparation and application. *Mater. Res. Express* **2022**, *9*, 015003. [[CrossRef](#)]
98. Cabrera, J.N.; Ruiz, M.M.; Fascio, M.; D'Accorso, N.; Minchev, R.; Dubois, P.; Lizarraga, L.; Negri, R.M. Increased surface roughness in polydimethylsiloxane films by physical and chemical methods. *Polymers* **2017**, *9*, 331. [[CrossRef](#)]
99. Paula, M.; Diego, I.; Dionisio, R.; Vinhas, G.; Alves, S. Gamma irradiation effects on polycaprolactone/zinc oxide nanocomposite films. *Polímeros* **2019**, *29*, e2019014. [[CrossRef](#)]
100. Gain, O.; Espuche, E.; Pollet, E.; Alexandre, M.; Dubois, P. Gas barrier properties of poly( $\epsilon$ -caprolactone)/clay nanocomposites: Influence of the morphology and polymer/clay interactions. *J. Polym. Sci. Part B Polym. Phys.* **2005**, *43*, 205–214. [[CrossRef](#)]
101. Dumitriu, R.P.; Stoleru, E.; Mitchell, G.R.; Vasile, C.; Brebu, M. Bioactive Electrospun Fibers of Poly( $\epsilon$ -Caprolactone) Incorporating  $\alpha$ -Tocopherol for Food Packaging Applications. *Molecules* **2021**, *26*, 5498. [[CrossRef](#)]
102. Dai, L.; Li, R.; Liang, Y.; Liu, Y.; Zhang, W. Development of Pomegranate Peel Extract and Nano ZnO Co-Reinforced Polylactic Acid Film for Active Food Packaging. *Membranes* **2022**, *12*, 1108. [[CrossRef](#)] [[PubMed](#)]
103. Salevi, A.; Prieto, C.; Cabedo, L.; Nedovi, V.; Lagaron, J.M. Physicochemical, Antioxidant and Antimicrobial Properties of Electrospun Poly ( $\epsilon$ -caprolactone) Films Containing a Solid Dispersion of Sage (*Salvia officinalis* L.) Extract. *Nanomaterials* **2019**, *9*, 270. [[CrossRef](#)] [[PubMed](#)]
104. Xu, Y.; Xie, L.; Hou, T.; Wang, D.; Zhang, T.; Li, C. Preparation and Properties of Asymmetric Polyvinyl Pyrroli-Done/Polycaprolactone Composite Nanofiber Loaded with Tea Tree Extract. *Polymers* **2022**, *14*, 3714. [[CrossRef](#)] [[PubMed](#)]
105. Radisavljevic, A.; Stojanovic, D.B.; Petrovic, M. Electrospun polycaprolactone nanofibers functionalized with *Achillea millefolium* extract yield biomaterial with antibacterial, antioxidant and improved mechanical properties. *J. Biomed. Mater. Res. Part A* **2022**, *111*, 962–974. [[CrossRef](#)] [[PubMed](#)]
106. Paul, S.; Saikia, J.P.; Samdarshi, S.K.; Konwar, B.K. Investigation of antioxidant property of iron oxide particles by 1'-diphenylpicryl-hydrazyle (DPPH) method. *J. Magn. Magn. Mater.* **2009**, *321*, 3621–3623. [[CrossRef](#)]

**Disclaimer/Publisher's Note:** The statements, opinions and data contained in all publications are solely those of the individual author(s) and contributor(s) and not of MDPI and/or the editor(s). MDPI and/or the editor(s) disclaim responsibility for any injury to people or property resulting from any ideas, methods, instructions or products referred to in the content.